10-28-2004

The morphotropic phase boundary and dielectric properties of the xPb(Zr1/2Ti1/2)O3-(1–x)Pb(Ni1/3Nb2/3)O3 perovskite solid solution

Naratip Vittayakorn
Chiang Mai University

Gobwute Rujijanagul
Chiang Mai University

Xiaoli Tan
Iowa State University, xtan@iastate.edu

Meagen A. Marquardt
Iowa State University

David A. Hall
Iowa State University

The morphotropic phase boundary and dielectric properties of the xPb(Zr1/2Ti1/2)O3-(1–x)Pb(Ni1/3Nb2/3)O3 perovskite solid solution

Abstract
The solid solution between the normal ferroelectricPb(Zr1/2Ti1/2)O3(PZT) and relaxor ferroelectricPb(Ni1/3Nb2/3)O3 (PNN) was synthesized by the columbite method. The phase structure and dielectric properties of xPZT-(1–x)PNN where x=0.4–0.9and the Zr/Ti composition was fixed close to the morphotropic phase boundary (MPB) were investigated. With these data, the ferroelectric phase diagram between PZT and PNN has been established. The relaxor ferroelectric nature of PNN gradually transformed towards a normal ferroelectric state towards the composition 0.7PZT-0.3PNN, in which the permittivity was characterized by a sharp peak and the disappearance of dispersive behavior. X-ray diffraction analysis demonstrated the coexistence of both the rhombohedral and tetragonal phases at the composition 0.8PZT-0.2PNN, a new morphotropic phase boundary within this system. Examination of the dielectric spectra indicates that PZT-PNN exhibits an extremely high relative permittivity near the MPB composition. The permittivity shows a shoulder at the rhombohedral to tetragonal phase transition temperature TRT=195°C, and then a maximum permittivity (36 000 at 10kHz) at the transition temperature Tmax=277°C at the MPB composition. The maximum transition temperature of this system was 326°C at the composition x=0.9 with the relative permittivity of 32 000 at 10kHz.

Keywords
Lead, Ozone, Relaxor ferroelectrics, Lead zirconate titanate, Permittivity, Niobium, Nickel, Ferroelectric phase transitions, X-ray diffraction, Solid solutions

Disciplines
Materials Science and Engineering

Comments
The following article appeared in *Journal of Applied Physics* 96 (2004): 5103 and may be found at http://dx.doi.org/10.1063/1.1796511.

The morphotropic phase boundary and dielectric properties of the x Pb (Zr 1 2 Ti 1 2) O 3 - (1 x) Pb (Ni 1 3 Nb 2 3) O 3 perovskite solid solution

Naratip Vittayakorn, Gobwute Rujijanagul, Xiaoli Tan, Meagen A. Marquardt, and David P. Cann

Citation: Journal of Applied Physics **96**, 5103 (2004); doi: 10.1063/1.1796511
View online: http://dx.doi.org/10.1063/1.1796511
View Table of Contents: http://scitation.aip.org/content/aip/journal/jap/96/9?ver=pdfcov
Published by the AIP Publishing

The morphotropic phase boundary and dielectric properties of the xPb($Zr_{1/2}Ti_{1/2}$)O_3-(1−x)Pb($Ni_{1/3}Nb_{2/3}$)O_3 perovskite solid solution

Naratip Vittayakorn and Gobwute Rujijanagul
Department of Physics Faculty of Science, Chiang Mai University, Chiang Mai 50200, Thailand

Xiaoli Tan, Meagen A. Marquardt, and David P. Cann
Materials Science and Engineering Department, Iowa State University, Ames, Iowa 50011

(Received 12 March 2004; accepted 30 July 2004)

The solid solution between the normal ferroelectric Pb($Zr_{1/2}Ti_{1/2}$)O_3 (PZT) and relaxor ferroelectric Pb($Ni_{1/3}Nb_{2/3}$)O_3 (PNN) was synthesized by the columbite method. The phase structure and dielectric properties of xPZT-(1−x)PNN where x=0.4–0.9 and the Zr/Ti composition was fixed close to the morphotropic phase boundary (MPB) were investigated. With these data, the ferroelectric phase diagram between PZT and PNN has been established. The relaxor ferroelectric nature of PNN gradually transformed towards a normal ferroelectric state towards the composition 0.7PZT-0.3PNN, in which the permittivity was characterized by a sharp peak and the disappearance of dispersive behavior. X-ray diffraction analysis demonstrated the coexistence of both the rhombohedral and tetragonal phases at the composition 0.8PZT-0.2PNN, a new morphotropic phase boundary within this system. Examination of the dielectric spectra indicates that PZT-PNN exhibits an extremely high relative permittivity near the MPB composition. The permittivity shows a shoulder at the rhombohedral to tetragonal phase transition temperature T_{RT}=195 °C, and then a maximum permittivity (36 000 at 10 kHz) at the transition temperature T_{max}=277 °C at the MPB composition. The maximum transition temperature of this system was 326 °C at the composition x=0.9 with the relative permittivity of 32 000 at 10 kHz. © *2004 American Institute of Physics*. [DOI: 10.1063/1.1796511]

I. INTRODUCTION

The relaxor ferroelectric lead nickel niobate [Pb($Ni_{1/3}Nb_{2/3}$)O_3, PNN] has been studied by numerous researchers since its discovery by Smolenskii and Agranovskaya in 1958.[1] At room temperature, single crystal PNN has the cubic prototype symmetry $Pm3m$ with a lattice parameter (a)=4.03 Å.[2] Nanometer-level chemical heterogeneity in the form of short range ordering of Ni^{2+} and Nb^{5+} on the B site was proposed to account for the diffuse phase transition.[3] The complex perovskite shows a broad maximum of the dielectric permittivity near −120 °C with relative permittivity near 4000 at 1 kHz.[4]

In the last decade, normal ferroelectric lead zirconate titanate [Pb($Zr_{1-x}Ti_x$)O_3, PZT] has become one of the most important commercially produced piezoelectric materials.[5,6] Excellent piezoelectric properties have been observed in compositions close to the morphotropic phase boundary (MPB Zr:Ti ~52:48).[5–7] Recently, many piezoelectric ceramic materials have been developed from binary systems containing a combination of relaxor and normal ferroelectric materials[8] which yield high dielectric permittivities (e.g., Pb($Mg_{1/3}Nb_{2/3}$)O_3-$PbTiO_3$,[9] Pb($Zn_{1/3}Nb_{2/3}$)O_3-$PbTiO_3$,[10,11] Pb($Mg_{1/3}Nb_{2/3}$)O_3-Pb(Zr,Ti)O_3,[12] excellent piezoelectric coefficients (e.g., Pb($Zn_{1/3}Nb_{2/3}$)O_3-$PbTiO_3$,[10,11] Pb($Zn_{1/3}Nb_{2/3}$)O_3-Pb(Zr,Ti)O_3,[13] Pb($Sc_{1/2}Nb_{1/2}$)O_3-$PbTiO_3$[14,15] and high pyroelectric coefficients (e.g., Pb($Ni_{1/3}Nb_{2/3}$)O_3-$PbTiO_3$-$PbZrO_3$).[16]

Fan and Kim[13] investigated the solid solution within the PZN-PZT binary system in which the Zr/Ti composition was close to the MPB. This study indicated that the composition 0.5PZN-0.5PZT showed the optimal piezoelectric properties. Moreover, these properties could be improved by thermal treatments. In 1974 Luff *et al.*[16] investigated solid solution in the Pb($Ni_{1/3}Nb_{2/3}$)O_3-$PbZrO_3$-$PbTiO_3$ ternary system and observed excellent piezoelectric properties at the composition 0.5Pb($Ni_{1/3}Nb_{2/3}$)O_3-0.35$PbTiO_3$-0.15$PbZrO_3$. There have been numerous papers published dealing with piezoelectric and processing issues within this compositional family.[16–19] These compositions have found wide applications and are now commercially available. However, there is limited information in the literature on the PNN-PZT system with Zr/Ti close to the MPB. Detailed reaction kinetics using conventional solid state processing of Pb($Ni_{1/3}Nb_{2/3}$)O_3-Pb($Zr_{0.48}Ti_{0.52}$)O_3 was recently investigated by Babushkin *et al.*.[20] A sequence of pyrochlore phases were detected at different temperatures, but there is no information pertaining to the dielectric and ferroelectric properties.

Since PNN is a relaxor ferroelectrics with a broad dielectric peak near $T_c \approx -120$ °C and PZT (Zr/Ti=50/50) is a normal ferroelectric with a sharp maximum permittivity at $T_c \sim 390$ °C, the curie temperature in PNN-PZT system can be engineered over a wide range of temperature by controlling the amount of PZT in the system. The aim of this work was to investigate the quasibinary solid solution xPZT (Zr/Ti=50/50)-(1−x)PNN, with x=0.4–0.9. Figure 1 schematically shows the pseudoternary composition range which

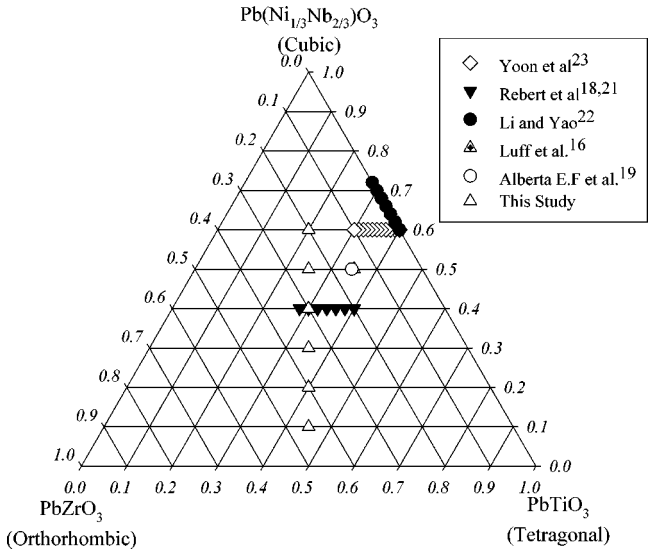

FIG. 1. Compositions studied in the $Pb(Ni_{1/3}Nb_{2/3})O_3$-$PbZrO_3$-$PbTiO_3$ ternary system.

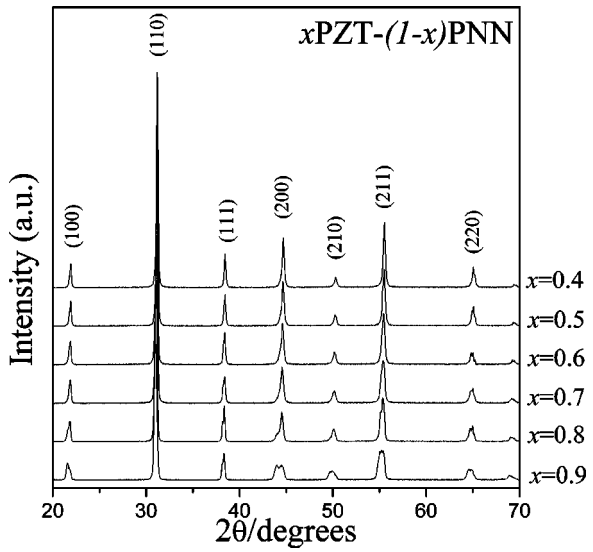

FIG. 2. XRD patterns at room temperature for xPZT-$(1-x)$PNN ceramics.

was studied in this work compared with other studies.[16,19–23] Although pure $Pb(Ni_{1/3}Nb_{2/3})O_3$-$PbZrO_3$-$PbTiO_3$ ternary ceramics can be fabricated by conventional methods,[16] the *B*-site precursor method is a better method for enhancing the dielectric properties and ferroelectric properties. This process involves prereacting the *B*-site cations to form the columbite phase $NiNb_2O_6$ and the wolframite phase $ZrTiO_4$. With this method it is possible to obtain a homogeneous perovskite solid solution without the other constituent perovskite phases such as $PbZrO_3$, $PbTiO_3$, PZT, PNN, and the formation of the parasitic pyrochlore phases is prevented. Finally, the nature of the relaxor-normal ferroelectric phase transition was studied through a combination of dielectric measurements and x-ray diffraction.

II. EXPERIMENT

The powders of xPZT-$(1-x)$PNN were synthesized using the columbite precursor method. Reagent-grade oxide powders of PbO, ZrO_2, TiO_2, NiO, and Nb_2O_5 were used as raw materials. The columbite structure ($NiNb_2O_6$) and wolframite structure ($ZrTiO_4$) were synthesized first. Stoichiometric amounts of the precursors (NiO, Nb_2O_5) and (ZrO_2, TiO_2) were mixed and milled in ethyl alcohol for 6 h using a vibratory mill. The mixture was dried at 60 °C for 12 h. The precursors $NiNb_2O_6$ and $ZrTiO_4$ were calcined at 975 °C and 1400 °C, respectively, for 4 h in a closed alumina crucible. The calcined $NiNb_2O_6$ and $ZrTiO_4$ powders were mixed with PbO in a stoichiometric ratio to form the composition xPZT-$(1-x)$PNN, where $x=0.4-0.9$ (shown in Fig. 1). In all compositions, 2 mol % excess PbO was added to compensate for lead volatilization during calcination and sintering. After remilling and drying, the mixtures were calcined at 950 °C for 4 h in a double alumina crucible configuration with a heating rate of 10 °C/min.

The calcined powders were milled for 3 h for reduced particle size. After grinding and sieving, the calcined powder was mixed with 5 wt % poly(vinyl alcohol) binder and uniaxially pressed into a pellet. Binder burnout occurred by slowly heating to 500 °C and holding for 2 h. Sintering occurred between 1100–1250 °C with a dwell time of 4 h. To mitigate the effects of lead loss during sintering, the pellets were sintered in a closed alumina crucible containing $PbZrO_3$ powder.

The perovskite phase was examined by x-ray diffraction (XRD). Data collection was performed in the 2 θ range of 20°–70° using step scanning with a step size of 0.02° and counting time of 2 s/step.

After surface grinding, the samples were electroded using sputtered gold and air-dried silver paint. The relative permittivity (ε_r) and dissipation factor ($\tan\delta$) were measured using an automated measurement system. This system consisted of an LCR meter (HP-4284A, Hewlett-Packard Inc.) in connection with a Delta Design 9023 temperature chamber and a sample holder (Norwegian Electroceramics) capable of high temperature measurement. The capacitance and dissipation factors of sample were measured at 100 Hz, 1 kHz, 10 kHz, and 100 kHz and temperature varied between 25–450 °C. A heating rate of 3 °C/min was used during measurements.

Samples were prepared for optical analysis by polishing with SiC paper through 1200 grit. Raman spectra were measured using a Renishaw inVia Reflex Raman microscope and 488 nm radiation from a laser excitation source. The laser had an output power of 25 mW and a focused spot size of 200–300 μm through a 5x microscope objective. Raman spectra were measured using a static acquisition centered at 520 cm^{-1} and 15 accumulations with 2 sec exposure times.

III. RESULTS AND DISCUSSION

A. Crystal structure and phase transition studies

Perovskite phase formation, crystal structure, and lattice parameter were determined by XRD at room temperature as a function of x. Figure 2 shows XRD patterns of ceramics in the xPZT-$(1-x)$PNN system with a well crystallized perovskite structure for all compositions. The pyrochlore phase was not observed for any composition in this system. The

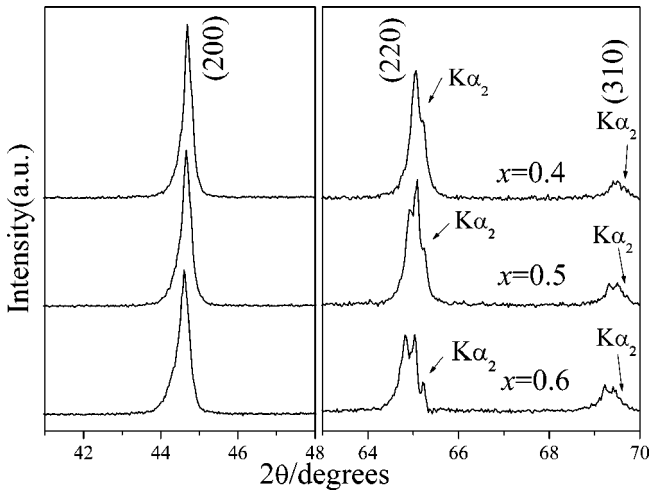

FIG. 3. XRD patterns of the (200) and (220) peaks of xPZT-$(1-x)$PNN ceramics, $x=0.4-0.6$.

crystal symmetry for pure PNN at room temperature is cubic $Pm3m$ with a lattice parameter $a=4.031$ Å. Below $T_{\max} \approx -120$ °C, the symmetry changes to rhombohedral. The crystal structure of $Pb(Zr_{1/2}Ti_{1/2})O_3$ at room temperature is tetragonal. Therefore, with increasing x the crystal symmetry should change due to the effects of the increased PZT fraction and the increase in T_C. Figure 3 shows XRD peak profiles of the (200) and (220) peaks at $x=0.4$, 0.5, and 0.6. The XRD data shows that the splitting of (200) peak is not observed. At the $x=0.4$ composition, only a single (220) peak is seen, indicating that the major phase in this composition had cubic symmetry. However, splitting was very clearly observed for the (220) peak in compositions $x=0.5$ and 0.6, indicating that the crystal transformed into rhombohedral symmetry (pseudocubic). With a further increase in PZT content to $x>0.6$, the (111) and (200) diffraction peaks begin to split as shown in Fig. 4. Splitting of the (200) peak becomes more pronounced as x approaches 0.9 indicating a stabilization of the tetragonal phase at high PZT concentrations.

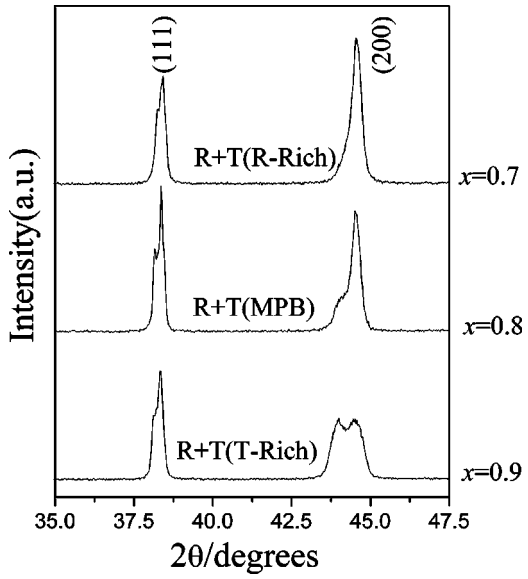

FIG. 4. XRD patterns of the (111) and (200) peaks of xPZT-$(1-x)$PNN ceramics, $x=0.7-0.9$.

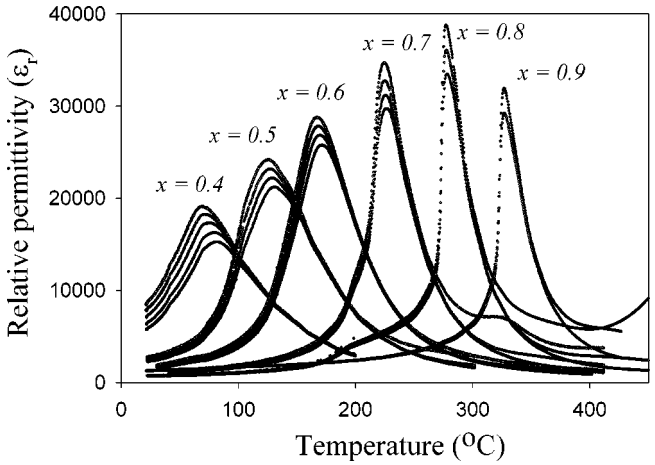

FIG. 5. Temperature dependence of the relative permittivity ε_r for xPZT-$(1-x)$PNN ceramics, $x=0.4-0.9$. Measurement frequencies include 100 Hz, 1 kHz, 10 kHz, and 100 kHz.

At the $x=0.8$ composition, the unambiguous splitting of (111) peak indicates the coexistence of the rhombohedral and tetragonal phase. Thus there is a transformation from the rhombohedral phase to the tetragonal phase across the compositional range $x=0.7-0.9$. The $x=0.7$ composition is within the rhombohedral-rich side of the MPB and the composition $x=0.9$ is on the tetragonal-rich side of the MPB. It is important to note that recent results have uncovered the existence of a low-symmetry (monoclinic) phase within the MPB region of PZT,[24] $Pb(Mg_{1/3}Nb_{2/3})O_3$-$PbTiO_3$[25] and the orthorhombic phase of $Pb(Zn_{1/3}Nb_{2/3})O_3$-$PbTiO_3$.[26] Given the similarities of PNN-PZT to the $Pb(Mg_{1/3}Nb_{2/3})O_3$-$PbTiO_3$ system, it is possible that a low symmetry monoclinic or orthorhombic phase may be stabilized within the MPB regions of xPZT-$(1-x)$PNN; $x=0.7-0.9$.

B. Dielectric properties

The characteristic temperature and frequency dependence of the relative permittivity for xPZT-$(1-x)$PNN, $x=0.4-0.9$, is shown in Fig. 5. A clear transition in $T_{\max}$ (defined as the temperature at which ε_r is maximum at 10 kHz) is observed with $T_{\max}$ increasing with x. At compositions $x=0.4$, 0.5, and 0.6, the sample displays a pronounced relaxor ferroelectric behavior, characterized by diffuse permittivity peaks and a shift of the maximum permittivity to higher temperatures with increasing frequency. An increase in the magnitude of the maximum permittivity is also observed over this region. The nature of the homogeneously polarized states is believed to be controlled by the concentration of PZT.

A smooth transition from relaxor to normal ferroelectric behavior is observed with increasing mole percent of PZT from $x=0.7$ to 0.9. This transition is characterized by the enhancement of the first-order nature of the phase transformation and the diminishment of the relaxor behavior (i.e., the permittivity dispersion) over the broad temperature range in the vicinity of $T_{\max}$. From these data, the relaxor-normal transformation is very clearly observed with increased PZT concentration above $x=0.7$. Furthermore, the relative permittivity and $T_{\max}$ increased with increased mole percent of PZT

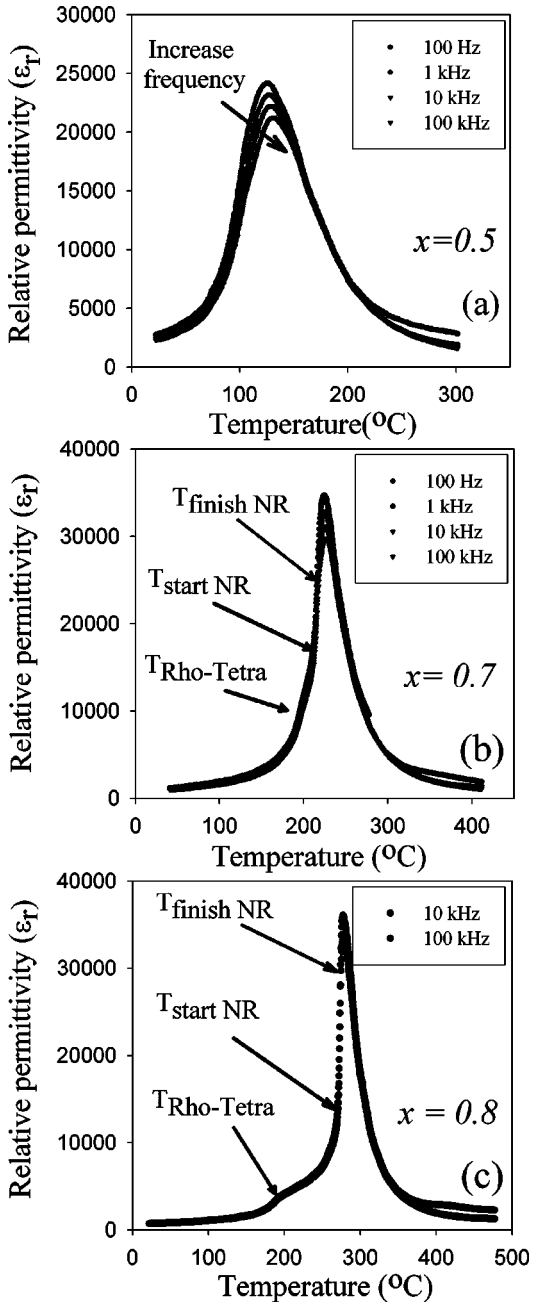

FIG. 6. Temperature dependence of the relative permittivity ε_r for xPZT-$(1-x)$PNN ceramics, A:$x=0.5$, B:$x=0.7$, and C:$x=0.8$.

considerably up to a maximum permittivity at $x=0.8$. The sharp permittivity peak exhibits a maximum value of 36 000 at 10 kHz for this composition. Figure 6 shows a comparison of the permittivity as a function of temperature for the compositions $x=0.5$, 0.7, and 0.8 taken over the measurement frequencies of 100 Hz–100 kHz.

For $x=0.5$, T_{max} increases from 125.6 °C at 100 Hz to 130.8 °C at 100 kHz ($\Delta T=5.2$ °C). The relative permittivity at room temperature was 2830 at 100 Hz and increased to 24 200 at 1 kHz at T_{max} and the maximum value of the relative permittivity decreased with increasing frequency. The dielectric dispersion below T_{max} indicates typical relaxor ferroelectric behavior arising from the responses of polar microdomains within the spectrum of the relaxation time. For $x=0.7$ and 0.8 compositions, it is evident that two phase transitions are observed. Over the temperature range 190 to 200 °C, a rhombohedral to tetragonal phase transition is observed for both compositions (indicated in the figure by $T_{\text{Rho-Tetra}}$). Another transition between the ferroelectric tetragonal to paraelectric cubic phase occurs in the temperature ranges 225 °C and 277 °C for $x=0.7$ and $x=0.8$, respectively. Although the transition from ferroelectric rhombohedral to tetragonal phase is obscured in the composition $x=0.7$ it is more clearly evident in the composition $x=0.8$. Similar phenomena has been observed in single crystal $Pb(Zn_{1/3}Nb_{2/3})O_3$-$PbTiO_3$,[11] $Pb(In_{1/2}Nb_{1/2})O_3$-$PbTiO_3$,[27] and $Pb(Mg_{1/3}Nb_{2/3})O_3$-$PbTiO_3$.[9]

In addition, the transformation from the relaxor ferroelectric state to the normal ferroelectric state can be observed in the composition $x=0.7-0.9$ as shown in Figs. 5, 6(b), and 6(c). The permittivity sharply increased near the temperature indicated as $T_{\text{start NR}}$ in Figs. 6(b) and 6(c). The subscript "start NR" denotes the initial transition from a normal ferroelectric state to a pure relaxor ferroelectric state. Relaxor behavior was observed at temperatures above $T_{\text{finish NR}}$. The subscript "finish NR" denotes the completion of the transformation. For $x=0.7$ at temperatures below 212 °C, the relative permittivity did not show any significant dispersion until 218 °C. Above this temperature, the relative permittivity shows a strong frequency dependence. This indicates that at 212 °C 0.7PZT-0.3PNN started to transform a normal ferroelectric state to relaxor ferroelectric state; finishing the transformation at 218 °C. The differential between $T_{\text{start NR}}$ and $T_{\text{finish NR}}$ was approximately 6 °C, 5 °C, and 4 °C for $x=0.7$, 0.8, and 0.9 respectively. This behavior can be explained by decreasing relaxor stability with increasing x.

At the composition $x=0.9$, a broad permittivity was observed with a slight frequency dispersion close to T_{max}. A first-order transition response was observed at temperatures slightly below T_{max}. This phenomenon indicates that the polar moments are static, since the polar moments are relatively large. The crystal structure and dielectric properties for all compositions are listed in Table I.

The maximum permittivity $\varepsilon_{r,max}$ and T_{max} as a function of the mole fraction of PZT(x) are represented in Fig. 7. There is a good linear relationship between T_{max} and x, indicating that this system is a well behaved complete solid solution. The T_{max} of the constituent compounds PNN and PZT are −120 °C and 390 °C, respectively, which can be used to calculate an empirical estimate of T_{max} via the equation,

$$T_{max} = x(390\ ^\circ\text{C}) + (1-x)(-120\ ^\circ\text{C}) \quad (1)$$

The variation of the measured T_{max}, the calculated T_{max}, and the measured $\varepsilon_{r,max}$ as a function of composition x is shown in Fig. 7. The highest $\varepsilon_{r,max}$ of 36 000 at 277 °C at 10 kHz was observed for the composition at the MPB 0.8PZT-0.2PNN. It is evident from the data that Eq. (1) gives a reasonable approximation of the transition temperature T_{max}. This result suggests that the transition temperature of xPZT-$(1-x)$PNN system can be varied over a wide range from −120 to 390 °C by controlling the amount of PZT in the system.

TABLE I. Ferroelectric properties of xPZT-$(1-x)$PNN ceramics (C, cubic; R, rhombohedral; T, tetragonal).

Composition x	Crystal structure	T_m(°C) at 10 kHz	Relative permittivity at 25 °C	Relative permittivity at T_{max}	tan δ at 25 °C	tan δ at T_m	δ_γ
$x=0.4$	C	75.4	7500	17 500	0.062	0.036	29.5
$x=0.5$	R	128.9	2500	22 000	0.042	0.024	24.4
$x=0.6$	R	169.7	1600	27 000	0.042	0.018	22.4
$x=0.7$	R-rich	225.5	1060	31 200	0.029	0.025	14.0
$x=0.8$	R+T	277.4	835	36 000	0.011	0.047	10.2
$x=0.9$	T-rich	326.7	950	32 000	0.005	0.182	8.6

It is well known that the permittivity of a first-order normal ferroelectric can be described by the Curie-Weiss law:

$$\frac{1}{\varepsilon_r} = \frac{T-\theta}{C}, \tag{2}$$

where θ is the Curie-Weiss temperature and C is Curie constant. A second-order relaxor ferroelectric can be described by a simple quadratic law. This arises from the fact that the total number of relaxors contributing to the permittivity response in the vicinity of the permittivity peak is temperature dependent, and the temperature distribution of this number is given by a Gaussian function about a mean value T_o with a standard deviation δ. The relative permittivity can be derived via the following expression:[28,29]

$$\frac{\varepsilon'_m}{\varepsilon'(f,T)} = 1 + \frac{[T-T_m(f)]^\gamma}{2\delta_\gamma^2} \quad (1 \leqslant \gamma \leqslant 2), \tag{3}$$

where ε'_m is the maximum value of the permittivity at $T=T_m(f)$. The value of γ is the expression of the degree of dielectric relaxation in the relaxor ferroelectric material. When $\gamma=1$ Eq. (3) expresses Curie-Weiss behavior, while for $\gamma=2$ this equation is identical to the quadratic relationship. Many relaxor ferroelectric materials can be fit to Eq. (3) with $\gamma=2$ at temperatures above T_{max}. The parameter δ_γ can be used to measure the degree of diffuseness of the phase transition in mixed relaxor-normal ferroelectric materials. The values γ and δ_γ are both material constants depending on the composition and structure of the material. The δ_γ value can be determined from the slope of $\varepsilon'_m/\varepsilon'$ versus $(T-T_m)^2$, which should be linear.

The δ_γ values of compositions in the xPZT-$(1-x)$PNN system are represented in Fig. 8. Both the diffuseness parameter δ_γ and γ decreased with an increase in the mole fraction of PZT. As illustrated in Fig. 9, a near linear relationship was observed over the wide compositional range, which is consistent with a perfect solid solution. The diffuseness of the phase transition in the $x=0.4$ composition can be attributed to the relaxor nature of PNN. As the PZT content increased, the relaxor characteristic of xPZT-$(1-x)$PNN was observed to decrease. This is because the substitution of $(Zr_{1/2}Ti_{1/2})^{4+}$ for the B-site complex ions $(Ni_{1/3}Nb_{2/3})^{4+}$ increases the size of the local polar domains by strengthening the off-center displacement and enhancing the interactions between micropolar domains. As was observed in $Pb(Mg_{1/3}Nb_{2/3})O_3$-$PbTiO_3$ crystals,[30] this leads to the formation of macropolar domains which break the symmetry of the pseudocubic state.

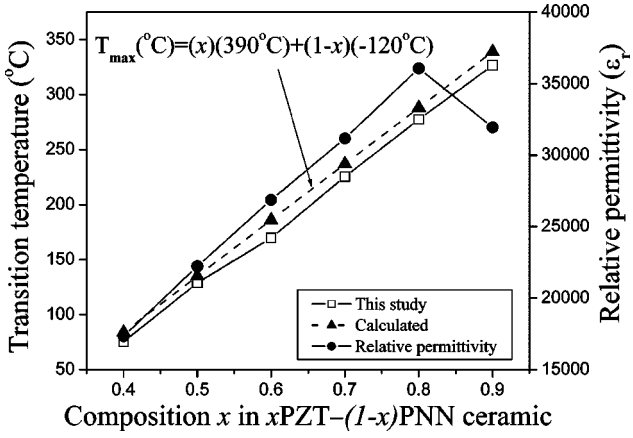

FIG. 7. T_{max}, calculated T_{max}, and maximum ε_r as a function of composition x at 10 kHz.

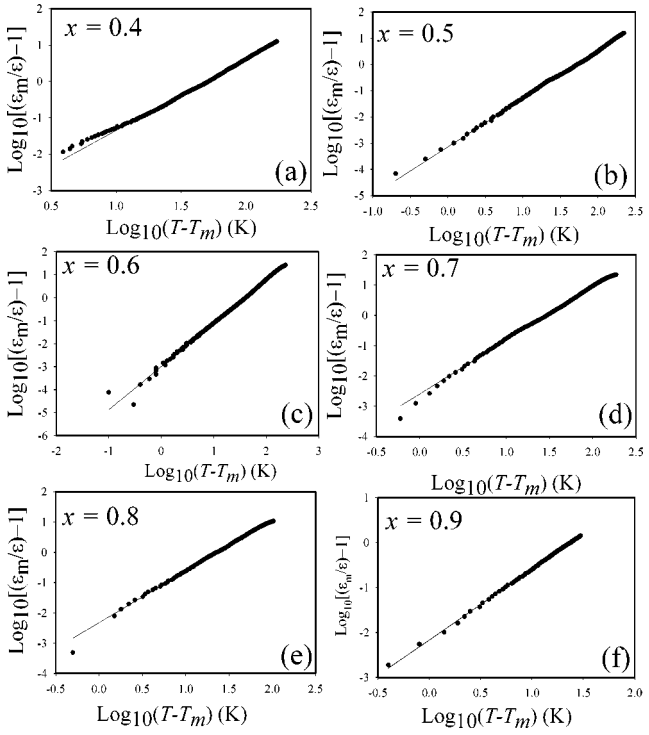

FIG. 8. $\mathrm{Log}_{10}[(\varepsilon_m/\varepsilon)-1]$ vs $\mathrm{Log}_{10}(T-T_{max})$ for xPZT-$(1-x)$PNN ceramics, $x=0.4-0.9$.

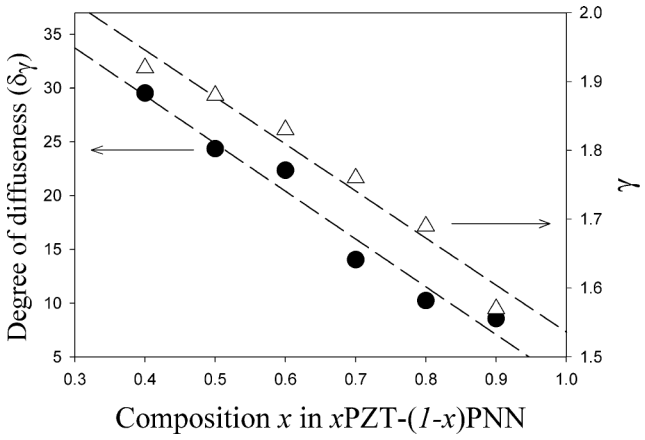

FIG. 9. Parameter γ and degree of diffuseness (δ_γ) vs x for xPZT-$(1-x)$PNN ceramics, $x=0.4-0.9$.

C. Raman spectroscopy of $Pb(Zr_{1/2}Ti_{1/2})O_3$-$Pb(Ni_{1/3}Nb_{2/3})O_3$

Figure 10 shows the Raman spectra of ceramic xPZT -$(1-x)$PNN with $x=0.4$ to 0.9. The individual spectral data was analyzed using Bruker Optics OPUS software. A multipeak pattern was fit to the data using Lorentz-Gauss peak shape parameters and Levenberg-Marquardt refinement techniques. The resulting peak locations for each xPZT-$(1-x)$PNN sample is shown in Fig. 11. Each peak represents a Raman active vibration mode frequency for the given composition. Peak location and intensity will vary depending on the type of bonds present in the material. There is a distinct difference in pattern when going from $x=0.4-0.5$. The disappearance of modes at 440 and 560 cm^{-1} and the appearance of modes at 675 and 890 cm^{-1} are indicative of a change in phase. The same is indicated for $x=0.7-0.8$, where a weak mode at 350 cm^{-1} first appears at $x=0.7$ and gains intensity for $x=0.8-0.9$. There is yet another change in mode pattern when going from $x=0.8-0.9$, where modes appear at 250, 670, and 834 cm^{-1}. These modes represent the splitting of a single mode for $x=0.8$.

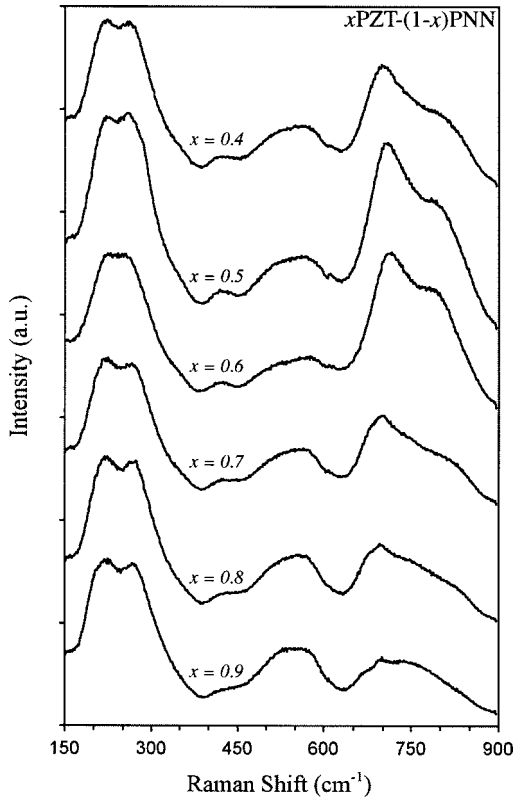

FIG. 10. Raman spectra of ceramic xPZT-$(1-x)$PNN with $x=0.4$ to 0.9.

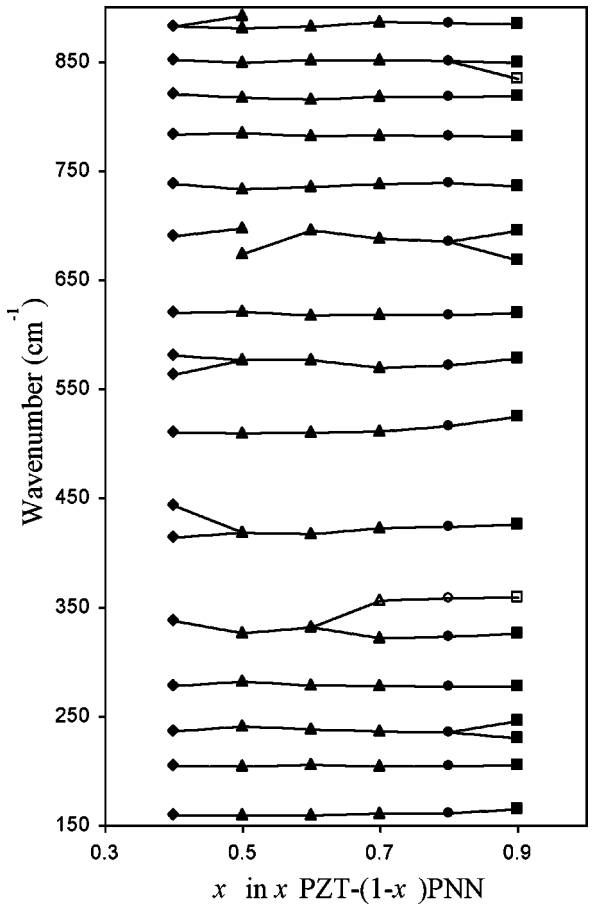

FIG. 11. Wave number as a function of composition x for ceramic xPZT-$(1-x)$PNN with $x=0.4$ to 0.9.

D. Phase diagram of $Pb(Zr_{1/2}Ti_{1/2})O_3$-$Pb(Ni_{1/3}Nb_{2/3})O_3$

Based on the results of x-ray diffraction, dielectric spectroscopy, and Raman spectroscopy, the phase diagram for the xPZT-$(1-x)$PNN binary system have been established as shown in Fig. 12. The transition temperature increases approximately linearly with x, from $T_{max}=75\,^{\circ}C$ for $x=0.4$ to $340\,^{\circ}C$ for $x=0.9$. The phase diagram consists of four distinct crystallographic phases in this system; high temperature paraelectric cubic ($Pm3m$), pseudocubic relaxor, rhombohedral relaxor ($R3m$), and normal ferroelectric tetragonal ($P4mm$). At low concentrations of PZT $x\leqslant 0.4$ the symmetry can be defined as pseudocubic. The pseudocubic symmetry transforms into rhombohedral at the composition near $x=0.5$. The ferroelectric rhombohedral and tetragonal phases are separated by an MPB region which is located near the composition $x=0.8$ below $277\,^{\circ}C$. Within this region, both the rhombohedral and tetragonal phases coexist. In most perovskite systems, the width of the MPB is limited though there may be low symmetry phases present.[24–26] In this work,

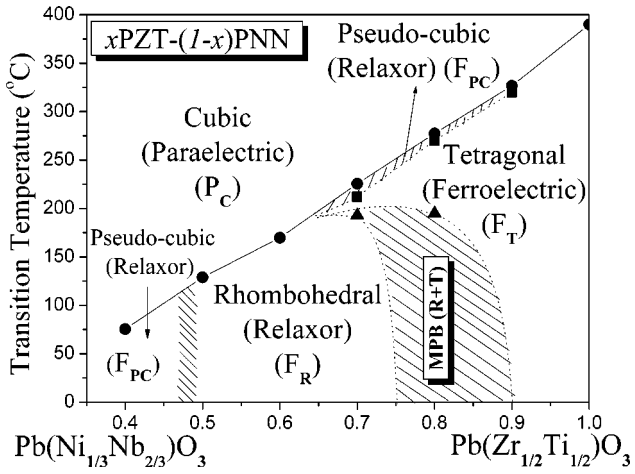

FIG. 12. Phase diagram of xPZT-$(1-x)$PNN, $x=0.4-0.9$ quasibinary system.

Fig. 12 shows the MPB region as broad because of the limited number of compositions in this study. Also, due to the nature of the ceramic preparation technique, mixed phases may be present within the MPB due to local compositional variations. Future work will be focused on identifying the width of the MPB and establishing the phase equilibria in the vicinity of the MPB.

IV. CONCLUSIONS

In this work the ferroelectric properties of the solid solution between relaxor ferroelectric PNN and normal ferroelectric PZT(50/50) have been investigated. The crystal structure data obtained from XRD indicates that the solid solution xPZT-$(1-x)$PNN, where $x=0.4-0.9$, successively transforms from pseudocubic to rhombohedral to tetragonal symmetry with an increase in PZT concentration. The XRD results were reinforced by Raman spectral analysis. The new MPB in this binary system is located near $x=0.8$, separating the rhombohedral and tetragonal phases. At the MPB composition, the permittivity exhibited a shoulder at $T_{RT}=195\ ^{\circ}C$ indicating a rhombohedral to tetragonal phase transformation with a maximum permittivity of 36 000 at 10 kHz at $T_{max}=277\ ^{\circ}C$. Moreover a transition from relaxor to normal ferroelectric behavior is clearly observed above a PZT concentration $x=0.7$. Furthermore, this transition between relaxor to normal ferroelectricity was typified by a quasilinear relationship between the diffuseness parameter δ_γ and PZT mole fraction x.

ACKNOWLEDGMENTS

The authors are grateful to the Thailand Research Fund (TRF), Graduate School of Chiang Mai University, and the Ministry of University Affairs for financial support.

[1]G. A. Smolenskii and A. L. Agranovskaya, Sov. Phys. Tech. Phys. **2**, 1380 (1958).
[2]V. A. Bokov and I. E. Myl'nikova, Sov. Phys. Solid State **3**, 613 (1961).
[3]C. A. Randall and A. S. Bhalla, Jpn. J. Appl. Phys., Part 1 **29**, 327 (1990).
[4]V. A. Bokov and I. E. Mylnikova, Sov. Phys. Solid State **2**, 2428 (1960).
[5]K. Uchino, *Ferroelectric Devices* (Marcel Dekker, New York, 2000).
[6]A. J. Moulson and J. M. Herbert, *Electroceramics Materials, Properties: Appications* (Chapman and Hall, New York, 1990).
[7]K. Uchino, Solid State Ionics **108**, 43 (1998).
[8]S. -E. Park and T. R. Shrout, IEEE Trans. Ultrason. Ferroelectr. Freq. Control **44**, 1140 (1997).
[9]T. R. Shrout, Z. P. Chang, N. Kim, and S. Markgraf, Ferroelectr., Lett. Sect. **12**, 63 (1990).
[10]J. Kuwata, K. Uchino, and S. Nomura, Ferroelectrics **37**, 579 (1981).
[11]M. L. Mulvihill, L. E. Cross, W. Cao, and K. Uchino, J. Am. Ceram. Soc. **80**, 1462 (1997).
[12]H. Ouchi, K. Nagano, and S. Hayakawa, J. Am. Ceram. Soc. **48**, T26–T31 (1965).
[13]H. Fan and H. E. Kim, J. Mater. Res. **17**, 180 (2002).
[14]Y. Yamashita, Jpn. J. Appl. Phys., Part 1 **33**, 4652 (1994).
[15]V. J. Tennery, K. W. Hang, and R. E. Novak, J. Am. Ceram. Soc. **51**, 671 (1968).
[16]D. Luff, R. Lane, K. R. Brown, and H. J. Marshallsay, Trans. J. Br. Ceram. Soc. **73**, 251 (1974).
[17]E. A. Buyanova, P. L. Strelets, I. A. Serova, and V. A. Isupov, Bull. Acad. Sci. USSR, Phys. Ser. (Engl. Transl.) **29**, 1877 (1965).
[18]G. Robert, M. Demartin, and D. Damjanovic, J. Am. Ceram. Soc. **81**, 749 (1998).
[19]E. F. Alberta and A. S. Bhalla, Int. J. Inorg. Mater. **3**, 987 (2001).
[20]O. Babushkin, T. Lindback, J. C. Luc, and J. Y. M. Leblais, J. Eur. Ceram. Soc. **18**, 737 (1998).
[21]G. Robert, M. D. Maeder, D. Damjanovic, and N. Setter, J. Am. Ceram. Soc. **84**, 2869 (2001).
[22]Z. Li and X. Yao, J. Mater. Sci. Lett. **20**, 273 (2001).
[23]M.-S. Yoon and H. M. Jang, J. Appl. Phys. **77**, 3991 (1995).
[24]B. Noheda, D. E. Cox, G. Shirane, J. A. Gonzalo, L. E. Cross, and S.-E. Park, Appl. Phys. Lett. **74**, 2059 (1999).
[25]Z.-G. Ye, B. Noheda, M. Dong, D. Cox, and G. Shirane, Phys. Rev. B **64**, 184114 (2001).
[26]D. La-Orauttapong, B. Noheda, Z.-G. Ye, P. M. Gehring, J. Toulouse, D. E. Cox, and G. Shirane, Phys. Rev. B **65**, 144101 (2002).
[27]Y. Guo, H. Luo, and T. He, Mater. Res. Bull. **38**, 85 (2003).
[28]H. T. Martirena and J. C. Burfoot, Ferroelectrics **7**, 151 (1974).
[29]K. Uchino and S. Nomura, Ferroelectr., Lett. Sect. **44**, 55 (1982).
[30]Z.-G. Ye and M. Dong, J. Appl. Phys. **87**, 2312 (2000).